

Probing the scotogenic FIMP at the LHC

Andre G. Hessler^{1*}, Alejandro Ibarra^{1†}, Emiliano Molinaro^{2‡}, and Stefan Vogl^{3,4§}

¹*Physik-Department T30d, Technische Universität München,
James-Frank-Straße, 85748 Garching, Germany*

²*CP³-Origins and University of Southern Denmark,
Campusvej 55, DK-5230 Odense M, Denmark*

³*Max Planck Institute for Nuclear Physics,
Saupfercheckweg 1, 69117 Heidelberg, Germany*

⁴*Institute for Nuclear Physics, Karlsruhe Institute of Technology,
Hermann-von-Helmholtz-Platz 1, 76344 Eggenstein-Leopoldshafen, Germany*

Abstract

We analyse the signatures at the Large Hadron Collider (LHC) of the scotogenic model, when the lightest Z_2 -odd particle is a singlet fermion and a feebly interacting massive particle (FIMP). We further assume that the singlet fermion constitutes the dark matter and that it is produced in the early Universe via the freeze-in mechanism. The small couplings required to reproduce the observed dark matter abundance translate into decay-lengths for the next-to-lightest Z_2 -odd particle which can be macroscopic, potentially leading to spectacular signatures at the LHC. We characterize the possible signals of the model according to the spectrum of the Z_2 -odd particles and we derive, for each of the cases, bounds on the parameters of the model from current searches.

1 Introduction

Understanding the nature of the dark matter of the Universe stands among the most pressing problems in Astroparticle Physics. A plausible hypothesis is that the dark matter is constituted by a population of new particles not contained in the Standard Model (for reviews, see [1, 2, 3]). Testing this hypothesis is, however, impeded by the vast number of dark matter candidates proposed in the literature, with very disparate characteristics and, correspondingly, with very different experimental signatures [4]. Over many years, the most popular and most studied dark matter candidate has been the Weakly Interacting Massive Particle

*andre.hessler@tum.de

†ibarra@tum.de

‡molinaro@cp3-origins.net

§stefan.vogl@mpi-hd.mpg.de

(WIMP) [5]. In this framework, the dark matter is assumed to be in thermal and chemical equilibrium with the plasma of Standard Model particles, and to become decoupled when the expansion rate becomes faster than the annihilation rate. If the strength of the WIMP interactions with the Standard Model particles is comparable to that of the weak interactions, the WIMP relic abundance is predicted to be in the ballpark of the observed dark matter abundance $\Omega h^2 \simeq 0.12$ [6]. The simplicity and economy of this framework has triggered enormous experimental efforts to detect non-gravitational WIMP signals. Unfortunately, no unambiguous signal has been found yet.

The lack of evidence for WIMP dark matter has prompted interest in other dark matter candidates and their identification, which usually requires search strategies very different to those for WIMPs. In this paper we concentrate on FIMPs as dark matter candidates [7]. FIMPs are characterized by a small interaction rate with the Standard Model particles, so that they never reach thermal equilibrium with the SM plasma throughout the whole cosmological history. However, they can be produced in decays and annihilations of Standard Model particles in the thermal bath, leading to a relic abundance which is essentially dictated by the time at which the expansion rate exceeded the production rate.

More concretely, we focus on a specific FIMP realization which may be linked to the mechanism of neutrino mass generation. We consider the scotogenic model [8], where the Standard Model particle content is extended by three fermion singlets and one scalar doublet. The model further assumes that the new particles are odd under a discrete Z_2 symmetry, assumed to be exactly conserved in the electroweak vacuum, while all the Standard Model particles are even. The lightest particle of the Z_2 -odd sector is absolutely stable and therefore constitutes a dark matter candidate. Several works have analysed the phenomenology of the scotogenic model when the dark matter candidate is a WIMP, which can be identified either with the lightest Z_2 -odd scalar [9] or with the lightest Z_2 -odd fermion [10]. In this work, in contrast, we will consider the scenario where the dark matter is a FIMP [11]. Due to the tiny strength of their interactions with ordinary matter, no observable signal is expected in direct and indirect search experiments. We will show in this paper that very distinctive signals may arise at the Large Hadron Collider, thus offering a promising avenue to test this model.

The paper is organized as follows. In Section 2 we review the main characteristics of the FIMP dark matter in the scotogenic model, in Section 3 we scrutinize the collider phenomenology of the model for three representative choices of the mass spectrum of the Z_2 -odd particles and in Section 4 we present our conclusions.

2 FIMP dark matter in the scotogenic model

In the scotogenic model [8], the particle content of the Standard Model (SM) is extended with one additional scalar doublet $H_2 \equiv (H^+, H_2^0)$ and three fermionic singlets N_j ($j = 1, 2, 3$). The model also postulates that the electroweak vacuum is invariant under a discrete Z_2 symmetry, under which all SM fields are even, whereas N_j and H_2 are odd. The Lagrangian of the model is given by

$$\mathcal{L} = \mathcal{L}_{\text{SM}} + \mathcal{L}_{H_2} + \mathcal{L}_N + \mathcal{L}_{\text{int}} , \quad (1)$$

where \mathcal{L}_{SM} denotes the SM Lagrangian, which includes the potential for the SM Higgs doublet H_1 ,

$$\mathcal{L}_{\text{SM}} \supset -\mu_1^2 (H_1^\dagger H_1) + \lambda_1 (H_1^\dagger H_1)^2, \quad (2)$$

\mathcal{L}_{H_2} and \mathcal{L}_N are, respectively, the terms in the Lagrangian involving only the fields H_2 and N_j ,

$$\mathcal{L}_{H_2} = (D_\mu H_2)^\dagger (D^\mu H_2) + \mu_2^2 (H_2^\dagger H_2) + \lambda_2 (H_2^\dagger H_2)^2, \quad (3)$$

$$\mathcal{L}_N = \frac{i}{2} \bar{N}_j \partial_\mu \gamma^\mu N_j - \frac{1}{2} M_j \bar{N}_j^c N_j + \text{h.c.}, \quad (4)$$

and \mathcal{L}_{int} contains the interaction terms of the Z_2 -odd fields with the Standard Model fields,

$$\begin{aligned} \mathcal{L}_{\text{int}} = & \lambda_3 (H_1^\dagger H_1) (H_2^\dagger H_2) + \lambda_4 (H_1^\dagger H_2) (H_2^\dagger H_1) + \frac{\lambda_5}{2} \left[(H_1^\dagger H_2)^2 + \text{h.c.} \right] \\ & + \left[Y_{\alpha i}^\nu (\bar{\nu}_{\alpha L} H_2^0 - \bar{\ell}_{\alpha L} H^+) N_i + \text{h.c.} \right]. \end{aligned} \quad (5)$$

The parameters of the scalar potential are chosen such that $\langle H_1 \rangle = (0, v/\sqrt{2})$, with $v \simeq 246$ GeV, and $\langle H_2 \rangle = 0$, hence the minimum of the potential breaks the electroweak symmetry while preserving the Z_2 symmetry.

The multiplet H_1 contains only one physical scalar state, the SM Higgs boson h , with $m_h = 125$ GeV [12, 13]. On the other hand, the Z_2 -odd scalar sector contains one CP-even (H^0), one CP-odd (A^0) and two charged (H^\pm) scalar fields, with masses

$$\begin{aligned} m_{H^0}^2 &= \mu_2^2 + v^2 (\lambda_3 + \lambda_4 + \lambda_5) / 2, \\ m_{A^0}^2 &= \mu_2^2 + v^2 (\lambda_3 + \lambda_4 - \lambda_5) / 2, \\ m_{H^\pm}^2 &= \mu_2^2 + v^2 \lambda_3 / 2, \end{aligned} \quad (6)$$

where μ_2 and $\lambda_{3,4,5}$ are couplings in the scalar potential.

The requirement of stability of the scalar potential further constrains the quartic couplings λ_k (see, e.g., [14]), which must satisfy the conditions

$$\begin{aligned} \lambda_{1,2} &> 0, \\ \lambda_3 &> -\sqrt{\lambda_1 \lambda_2}, \\ \lambda_3 + \lambda_4 \pm |\lambda_5| &> -\sqrt{\lambda_1 \lambda_2}. \end{aligned} \quad (7)$$

Additional relations involving different combinations of λ_k arise from perturbative partial-wave unitarity of tree-level scattering diagrams [15].

The model violates total lepton number and, in general, all three family lepton numbers. However, due to the assignment of the Z_2 charges, lepton and flavour violating processes involving only Standard Model particles in the initial and final states only arise at the one loop level, and thus with a suppressed rate. In particular, the model predicts non-vanishing neutrino masses. At lowest order in perturbation theory the neutrino mass term reads [8]:

$$(\mathcal{M}_\nu)_{\alpha\beta} = \sum_k \frac{Y_{\alpha k}^\nu Y_{\beta k}^\nu}{16 \pi^2} M_k \left[\frac{m_{H^0}^2}{m_{H^0}^2 - M_k^2} \log \left(\frac{m_{H^0}^2}{M_k^2} \right) - \frac{m_{A^0}^2}{m_{A^0}^2 - M_k^2} \log \left(\frac{m_{A^0}^2}{M_k^2} \right) \right]. \quad (8)$$

Small neutrino masses can be generated by *i*) postulating small Yukawa couplings, *ii*) postulating that the Z_2 -odd particles in the loop are heavy, *iii*) postulating that the quartic coupling λ_5 is very small. Of special interest is the scenario where the new particles responsible for neutrino masses have masses below the TeV scale and sizeable couplings with the Standard Model particles. If this is the case, the new particles could produce observable signals in experiments at the energy and the intensity frontiers, thus opening the exciting possibility of testing the model of neutrino mass generation. For $\lambda_5 \ll 1$ this expression simplifies and the mass matrix can be written as

$$(\mathcal{M}_\nu)_{\alpha\beta} \simeq \frac{\lambda_5 v^2}{16 \pi^2} \sum_k Y_{\alpha k}^\nu Y_{\beta k}^\nu \frac{M_k}{m_0^2 - M_k^2} \left(1 - \frac{M_k^2}{m_0^2 - M_k^2} \log \left(\frac{m_0^2}{M_k^2} \right) \right), \quad (9)$$

where $m_0^2 = (m_{H^0}^2 + m_{A^0}^2)/2$. This assumption implies in particular, $m_{H^0}^2 \simeq m_{A^0}^2$ and $m_{A^0}^2 - m_{H^\pm}^2 \simeq v^2 \lambda_4/2$, as follows from Eq. (6).

The rates for the charged lepton flavour violating processes also vanish at tree level, but are predicted to arise at the one loop level [10, 16]. The strongest limits on the model parameters follow from the current upper bound on the $\mu \rightarrow e \gamma$ branching ratio, $\text{BR}(\mu \rightarrow e \gamma) < 4.2 \times 10^{-13}$ at 90% CL [17]. In the scotogenic model, the branching ratio reads

$$\begin{aligned} \text{BR}(\mu \rightarrow e \gamma) &= \frac{3 \alpha_{\text{em}}}{64 \pi G_F^2 m_{H^\pm}^4} \left| \sum_k Y_{\mu k}^\nu Y_{ek}^{\nu *} F_2 \left(\frac{M_k^2}{m_{H^\pm}^2} \right) \right|^2 \\ &\approx 10^{-15} \left(\frac{100 \text{ GeV}}{m_{H^\pm}} \right)^4 \left| \frac{y_k}{10^{-2}} \right|^4 \left(\frac{F_2(M_k^2/m_{H^\pm}^2)}{3 \times 10^{-3}} \right)^2, \end{aligned} \quad (10)$$

where $y_k \equiv (\sum_\alpha |Y_{\alpha k}|^2)^{1/2}$, $k = 1, 2, 3$, and $F_2(x)$ is a monotonically decreasing loop function which varies between 0.14 and 3×10^{-5} for x between 0.1 and 10^4 .

The conservation of the Z_2 symmetry ensures that the lightest Z_2 -odd particle is absolutely stable, which then constitutes a dark matter candidate if it is electrically neutral. The dark matter candidates of the model are the CP-even and CP-odd neutral scalars, H^0 and A^0 , and the lightest singlet fermion N_1 . Here we focus on the latter candidate, the singlet fermion. The dark matter may be produced via the freeze-out mechanism, however this mechanism requires sizeable Yukawa couplings which generically lead to too large rates for the rare leptonic decays (see, however, [18]). In order to suppress the rare decays we assume that N_1 interacts very weakly with the Standard Model particles. The dark matter population can then be generated from the freeze-in mechanism [7] and from the decay of the next-to-lightest Z_2 -odd particle, dubbed superWIMP mechanism [19]. The latter contribution, on the other hand, can always be neglected if the scalar particles have a mass $m_{H_2} \lesssim 500 \text{ GeV}$ and $M_1 \lesssim 100 \text{ MeV}$ (see [11] for a detailed discussion).

In the following we will consider the region of the parameter space of the model where the observed dark matter abundance, $\Omega_{\text{DM}} h^2 \approx 0.12$, is entirely generated by the freeze-in mechanism. The dark matter density is approximately given by [11]

$$\Omega_{N_1} h^2 \approx 0.12 \left(\frac{M_1}{10 \text{ keV}} \right) \left(\frac{100 \text{ GeV}}{m_{H_2}} \right) \left(\frac{y_1}{2 \times 10^{-9}} \right)^2, \quad (11)$$

provided $|m_{H^0/A^0} - m_{H^\pm}| \lesssim 100 \text{ GeV}$, where m_{H_2} is the overall mass of the Z_2 -odd scalars. Therefore, a ballpark estimate of the size of the Yukawa couplings leading to the observed

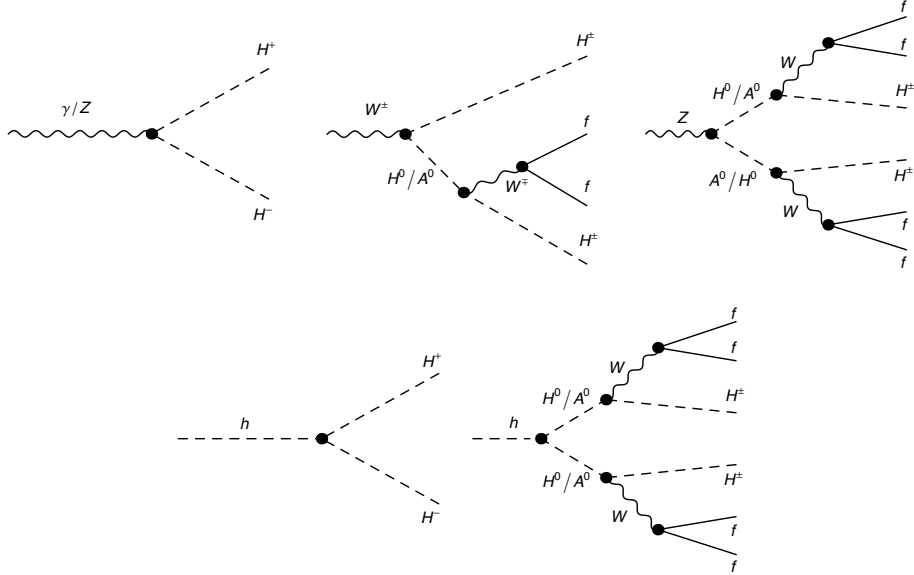


Figure 1: Drell-Yan (upper row) and gluon-gluon fusion (lower row) production channels of the Z_2 -odd charged scalar.

dark matter abundance via freeze-in is

$$y_1 \approx 2 \times 10^{-9} \left(\frac{10 \text{ keV}}{M_1} \right)^{1/2} \left(\frac{m_{H_2}}{100 \text{ GeV}} \right)^{1/2}. \quad (12)$$

The tiny Yukawa couplings required by the FIMP mechanism imply that the dark matter plays a subdominant role in the neutrino mass generation, which is then dominated by the heavier fermions $N_{2,3}$. The strength of their Yukawa interactions to the Standard Model is constrained from below by the requirement of correctly reproducing the measured neutrino parameters, and constrained from above by the experimental upper bound on $\text{BR}(\mu \rightarrow e\gamma)$. Postulating masses for the new particles below the TeV scale and assuming $\lambda_5 < 0.1$, one obtains

$$10^{-5} \lesssim y_{2,3} \lesssim 10^{-2}. \quad (13)$$

3 Collider phenomenology

FIMPs, due to their tiny interactions with the Standard Model particles, are not directly produced at colliders. However, they are produced in the decays of the Z_2 -odd scalars H^0 , A^0 and H^\pm , which can be copiously produced at the LHC via neutral and charged current Drell-Yan (DY) processes.¹ Here we assume for concreteness that $m_{H^\pm} < m_{H^0, A^0}$, corresponding to $\lambda_4 > 0$, such that the FIMP is dominantly produced in the decay $H^\pm \rightarrow N_1 \ell_\alpha^\pm$, where H^\pm can be produced either directly in the partonic collision, or in the decay $H^0/A^0 \rightarrow H^\pm W^\mp$. The dominant production channels for the charged scalar H^\pm are shown in Fig. 1. We remark

¹Under certain conditions gluon-gluon fusion (ggF) with an off-shell Higgs in the s-channel can also be relevant [20].

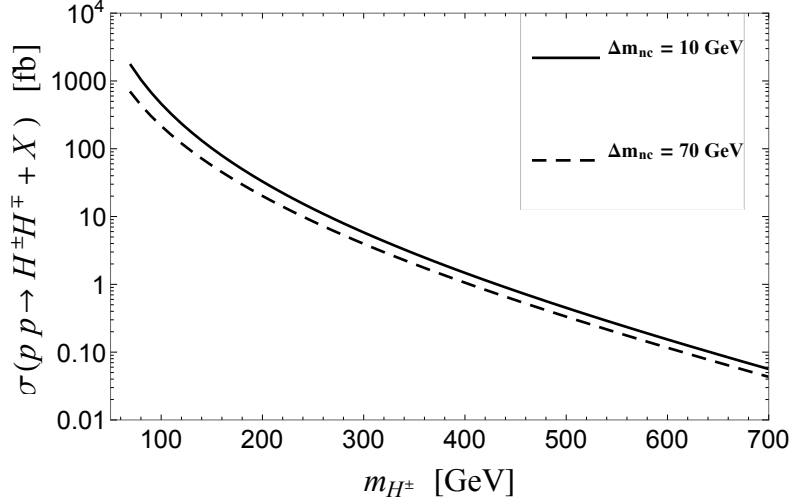


Figure 2: Drell-Yan production cross-sections at $\sqrt{s} = 8$ TeV for $\Delta m_{nc} = 10$ GeV (black solid line) and $\Delta m_{nc} = 70$ GeV (black dashed line).

that in the following we impose $\lambda_5 \ll 1$, therefore the decays $H^0/A^0 \rightarrow A^0/H^0 + Z^*$ are suppressed, and we neglect them in our analysis. The DY production cross-section of charged scalar pairs at the LHC, for a center-of-mass energy $\sqrt{s} = 8$ TeV, is reported in Fig. 2 for two benchmark scenarios, which are defined by the scalar mass splitting $\Delta m_{nc} \equiv m_{H^0/A^0} - m_{H^\pm}$, namely $\Delta m_{nc} = 10$ GeV (solid black line) and $\Delta m_{nc} = 70$ GeV (dashed black line).

At the LHC the signals of the scotogenic FIMP scenario crucially depend on the masses of the Z_2 -odd fermions relative to the Z_2 -odd scalars. We consider here the following three representative scenarios:

- Scenario A: $M_1 < m_{H^\pm, H^0, A^0} < M_{2,3}$
- Scenario B: $M_1 < M_2 < m_{H^\pm, H^0, A^0} < M_3$
- Scenario C: $M_1 < M_2 < M_3 < m_{H^\pm, H^0, A^0}$

with the mass ordering in the scalar sector $m_{H^\pm} < m_{H^0} \simeq m_{A^0}$, which corresponds, as indicated earlier, to $\lambda_5 \ll 1$ and $\lambda_4 > 0$. Let us discuss each of them separately.

3.1 Scenario A: $M_1 < m_{H^\pm, H^0, A^0} < M_{2,3}$

In this scenario, the charged scalar H^\pm can only decay into the FIMP and a charged lepton, with a rate given by [11]

$$\Gamma(H^\pm \rightarrow N_1 \ell_\alpha^\pm) = \frac{m_{H^\pm} |Y_{\alpha 1}^\nu|^2}{16\pi} \left(1 - \frac{M_1^2}{m_{H^+}^2}\right)^2 \approx \frac{m_{H^\pm} |Y_{\alpha 1}^\nu|^2}{16\pi}. \quad (14)$$

For FIMP dark matter, the proper decay-length of H^\pm , $c\tau(H^\pm)$, can be readily computed from Eqs. (14) and (12). The result is

$$c\tau(H^\pm) \approx 8.3 \text{ m} \left(\frac{M_1}{10 \text{ keV}} \right) \left(\frac{100 \text{ GeV}}{m_{H^\pm}} \right)^2 \quad (15)$$

and can clearly exceed the size of the ATLAS and CMS detectors.

The long decay-lengths expected for H^\pm result in a charged track signal when this particle traverses the inner detector and the muon system. As the H^\pm is very heavy compared to long-lived standard model particles, its momentum is comparatively low and, as a consequence, the amount of energy deposited in the detector is abnormally high. These features distinguish long-lived heavy charged particles from SM backgrounds, *i.e.* muons, thus allowing to define clean search regions by vetoing velocities close to the speed of light and by requiring a high ionization. The CMS collaboration has conducted a search for heavy stable charged particles creating such tracks [21], which was employed to derive constraints on the cross-section and the mass for selected benchmark scenarios. In Section 3.1.1, we recast this search taking into account that, for light dark matter, H^\pm may not traverse the whole detector (as implicitly assumed by the CMS analysis), but may instead decay into a FIMP and a charged lepton.

On the other hand, the charged scalars can be produced with such low momenta that they are stopped within the electromagnetic or hadronic calorimeters. Once trapped, they can decay at random times relatively to the trigger rate. When decaying during a time interval in which there is no bunch crossing, the signature can be a jet-like energy deposition that is largely free of backgrounds. The ATLAS collaboration conducted a search for stopped R-hadrons decaying out-of-time producing such signals [22]. Our study in Section 3.1.2 uses the provided efficiency for a decay event to pass the out-of-time trigger of ATLAS, in order to assess the sensitivity to signals caused by stopped H^\pm .

3.1.1 Charged-tracks analysis: in-flight decays of the Z_2 -odd charged scalar

To derive constraints on the scotogenic FIMP model, we employ the null results from the search for metastable singly-charged particles leaving the detector conducted by the CMS collaboration in [21], based on $L = 18.8 \text{ fb}^{-1}$ of data collected at $\sqrt{s} = 8 \text{ TeV}$. The number of expected events reads

$$N_{\text{exp}} = \sigma L \mathcal{A}, \quad (16)$$

where σ is the production cross-section and \mathcal{A} the signal acceptance. We determine \mathcal{A} for a given m_{H^\pm} and M_1 as described in [23] while taking the finite particle decay-length fully into account. The acceptances are computed with a detector simulation of Monte Carlo events imposing the same kinematical cuts ($|\eta| < 2.1$, $p_T > 45 \text{ GeV}$, $\beta < 0.95$) and isolation criteria as in [21]. In our treatment of the in-flight decays we approximate the geometry of the CMS detector by a barrel which covers the pseudorapidity range $0 \leq |\eta| < 1.2$ and has a radius $r = 738 \text{ cm}$, and endcaps covering $1.2 \leq \eta \leq 2.4$ which extend to $z = 975 \text{ cm}$ from the production point. The acceptance we obtain for different values of m_{H^\pm} is shown in Fig. 3, left panel, as a function of the FIMP mass for different values of m_{H^\pm} . As seen in the figure, the acceptance saturates for large M_1 , as practically all produced charged Z_2 -odd scalars leave the detector before decaying.

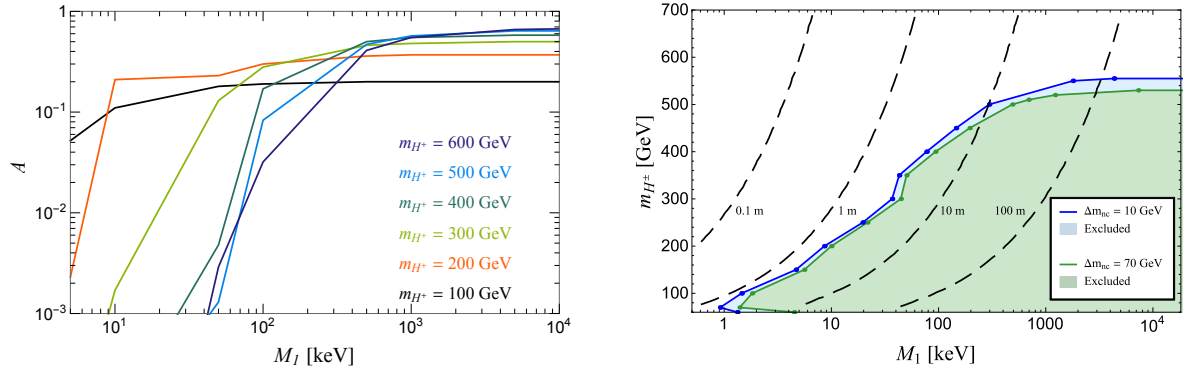


Figure 3: *Left panel:* Signal acceptance for the charged track analysis in Scenario A (see text for details), as a function of the FIMP mass for different values of the Z_2 -odd charged scalar mass, H^\pm . *Right panel:* Region of the parameter space excluded at 95% CL in Scenario A for $\Delta m_{\text{nc}} = 10$ (70) GeV; the long-dashed contour lines correspond to different values of the proper decay-length of H^\pm .

We consider two benchmark scenarios for the mass spectrum in the Z_2 -odd scalar sector, $\Delta m_{\text{nc}} = 10$ (70) GeV, with Drell-Yan production cross-sections σ given in Fig. 2 (gluon-gluon fusion contributes negligibly to this signature). Finally, and following the procedure described in [23], we confront the expected number of events with the observed number of events in the search regions $m_{H^\pm} < 166$ GeV, $166 \text{ GeV} < m_{H^\pm} < 330$ GeV, $330 \text{ GeV} < m_{H^\pm} < 500$ GeV and $m_{H^\pm} > 500$ GeV. The regions of the parameter space spanned by m_{H^\pm} and M_1 excluded by the CMS search are shown in Fig. 3, right panel. As apparent from the figure, for low M_1 this search is practically insensitive to the scotogenic FIMP model, since a significant fraction of the charged Z_2 -odd scalars decays inside the detector (contours of constant $c\tau$ are also shown in the plot, as long-dashed lines, for comparison). As M_1 increases, a larger and larger fraction of charged scalars leave the detector, thus strengthening the lower limit of m_{H^\pm} . The limit eventually saturates for $M_1 \gtrsim 10$ MeV, when practically all the charged scalars are stable within the detector. In this regime, one finds the lower bound $m_{H^\pm} \gtrsim 560$ (530) GeV for $\Delta m_{\text{nc}} = 10$ (70) GeV, regardless of the value of M_1 .

3.1.2 Decays of stopped long-lived Z_2 -odd charged scalars

If the charged scalar is produced with sufficiently low momentum, it may be stopped in the detector before decaying, producing a characteristic signal. We report in Fig. 4 the normalized differential cross section $\frac{1}{\sigma} \frac{d\sigma}{d\beta d\gamma}$ for H^\pm produced in proton-proton collisions at $\sqrt{s} = 8$ TeV for the benchmark mass $m_{H^\pm} = 150$ GeV, assuming $\Delta m_{\text{nc}} = 10$ GeV. We also show the fraction of particles which are produced from DY and from ggF via an off-shell Higgs, through the Lagrangian term $\mathcal{L} \supset -\lambda_3 v h H^\pm H^\mp$; the left panels show the results for $\lambda_3 = 1$ and the right panels for $\lambda_3 = 2$.² The distributions were obtained with CalcHEP [24].

²We have verified that this set of parameters is in agreement with constraints from $h \rightarrow \gamma\gamma$ (to which H^\pm contributes via a triangle loop), potential boundedness and unitarity of scalar scattering amplitudes.

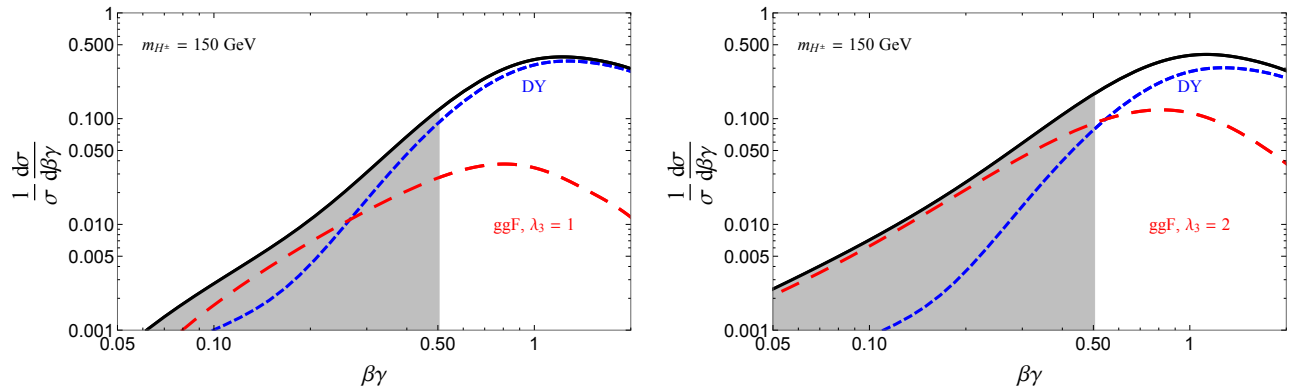


Figure 4: Contribution to the H^\pm distribution in $\beta\gamma$ from Drell-Yan and gluon-gluon fusion at $\sqrt{s} = 8$ TeV. We fix $m_{H^\pm}^\pm = 150$ GeV and $m_{H^0} = m_{A^0} = m_{H^\pm} + \Delta m_{\text{nc}}$, with $\Delta m_{\text{nc}} = 10$ GeV. The scalar quartic couplings in the left (right) panels are $\lambda_5 = 0$ and $\lambda_3 = +1$ ($+2$).

The grey shaded region in each plot shows the $\beta\gamma$ values for which the charged scalar particle will stop within the barrel region ($|\eta| < 1.2$) of the simplified ATLAS model employed in our analysis. The specifications of the detector are summarized in Tab. 1 in Appendix A. As can be seen, the ggF mechanism enhances the number of particles stopped within the detector for some choices of the parameters of the model even though the ggF contribution to the total cross-section remains subleading.

Among all the charged scalars produced, only a fraction will eventually be stopped in the detector. We determine the stopping efficiency, ϵ_{stop} , for different masses of H^\pm following the procedure detailed in Appendix A. For $\lambda_3 = 0$, we find $\epsilon_{\text{stop}} = 0.0076$ (0.0065) for $m_{H^\pm} = 150$ GeV and $\sqrt{s} = 7$ TeV (8 TeV). For non-vanishing λ_3 , the ggF channel increases the efficiency to $\epsilon_{\text{stop}} = 0.0095$ (0.0085) for a quartic coupling $\lambda_3 = 1$ and to $\epsilon_{\text{stop}} = 0.0129$ (0.0133) for $\lambda_3 = 2$. Once trapped, the charged scalars can decay at random times relative to the trigger rate. Searches for out-of-time decays are conducted in the time interval in which there is no bunch crossing. The timing acceptance $\epsilon_T(\tau)$ depends on the operation mode of the LHC, in particular the bunch structure, and was presented in Fig. 7 of [22]: $\epsilon_T(\tau)$ is identically zero for lifetimes $\tau \lesssim 10^{-7}$ s, then rises to a constant plateau of ≈ 0.08 starting at $\tau \approx 10^{-5}$ s and starts to decrease at $\tau \approx 10^3$ s. This implies, in particular, that this search is only sensitive for FIMP masses $M_1 \gtrsim 1$ MeV when $m_{H^\pm} \sim 100$ GeV, since for smaller masses the charged scalar lifetime is smaller than 10^{-7} s, for which the timing efficiency is zero.

The decay products can then be detected. We use the results of the search for stopped R-hadrons decaying out-of-time conducted by the ATLAS collaboration [22]. This search relies on the observation of jets. Consequently, it is only sensitive to events of the type $H^\pm \rightarrow N_1 \tau^\pm$ followed by $\tau^\pm \rightarrow \text{hadrons}$ and not to electrons or muons. Furthermore, the search is only sensitive to events with a leading jet energy $E > 50$ GeV. In order to estimate the effect of this cut, we simulate τ leptons from H^\pm decays at rest with Pythia8 [25] and use Delphes [26] to include detector effects. For $m_{H^\pm} > 300$ GeV, the reconstruction efficiency approaches the limit imposed by the leptonic branching fraction of the τ , and reads $\epsilon_{\text{rec}} = 0.65$. For lower masses, the efficiency substantially degrades, being $\epsilon_{\text{rec}} = 0.39$ (0.23)

for $m_{H^\pm} = 150$ (120) GeV. The number of expected events then reads:

$$N_{\text{exp}} = \sigma L \epsilon_{\text{stop}} \epsilon_{\text{rec}} \epsilon_T(\tau). \quad (17)$$

Assuming $\text{BR}(H^\pm \rightarrow \tau^\pm N_1) \approx 1$ and $\lambda_3 = 0$ we obtain $N_{\text{exp}} = 1.0$ (0.60) expected signal events for $m_{H^\pm} = 120$ GeV (150 GeV). For non-vanishing λ_3 , the total production cross-section is enhanced by the ggF mechanism, and the number of expected signal events increases to $N_{\text{exp}} = 1.3$ (0.78) for $\lambda_3 = 1$ and to $N_{\text{exp}} = 2.0$ (1.3) for $\lambda_3 = 2$.

The ATLAS search [22] found an event rate in agreement with the background expectation. Using the observed events and the background expectation in the search region with a leading jet energy larger than 50 GeV, one obtains, using the Feldman-Cousins procedure [27], an upper limit on the number of signal events of $N_{\text{sig}} \lesssim 4.3$. Due to the small expected signal, this search is therefore not sensitive enough to probe our scenario.

3.2 Scenario B: $M_1 < M_2 < m_{H^0, A^0, H^\pm} < M_3$

When N_2 is lighter than the Z_2 -odd scalars, the decay modes $H^\pm \rightarrow N_2 \ell_\alpha^\pm$ become kinematically allowed, with rate [11]:

$$\Gamma(H^\pm \rightarrow N_2 \ell_\alpha^\pm) = \frac{m_{H^\pm} |Y_{\alpha 2}^\nu|^2}{16\pi} \left(1 - \frac{M_2^2}{m_{H^\pm}^2}\right)^2 \approx \frac{m_{H^\pm} |Y_{\alpha 2}^\nu|^2}{16\pi}. \quad (18)$$

Neutrino oscillation data and the upper limit on $\text{BR}(\mu \rightarrow e\gamma)$ favour $y_2 \equiv (\sum_\alpha |Y_{\alpha 2}^\nu|^2)^{1/2}$ in the range $\sim 10^{-5} \div 10^{-2}$, *cf.* Eq. (13). Therefore H^\pm will dominantly decay into the next-to-lightest Z_2 -odd fermion, with a decay-length which is typically below 1 mm, while decays into N_1 are negligibly rare.

In this scenario, instead, FIMPs are dominantly produced in the decay of the next-to-lightest Z_2 -odd fermion, through $N_2 \rightarrow \ell_\alpha^- \ell_\beta^+ N_1$ and $N_2 \rightarrow \nu_\alpha \bar{\nu}_\beta N_1$. The rates for these processes read:

$$\Gamma(N_2 \rightarrow \ell_\alpha^- \ell_\beta^+ N_1) \simeq \Gamma(N_2 \rightarrow \nu_\alpha \bar{\nu}_\beta N_1) \simeq \frac{M_2^5}{6144 \pi^3 m_{H^\pm}^4} \left(|Y_{\beta 1}^\nu|^2 |Y_{\alpha 2}^\nu|^2 + |Y_{\alpha 1}^\nu|^2 |Y_{\beta 2}^\nu|^2 \right), \quad (19)$$

For the values of the FIMP coupling to the leptons required to correctly reproduce the observed dark matter abundance via freeze-in, Eq. (12), the decay-length in vacuum of N_2 is:

$$c\tau(N_2) \approx 2 \times 10^{13} \text{ m} \left(\frac{M_1}{10 \text{ keV}} \right) \left(\frac{m_H}{500 \text{ GeV}} \right)^3 \left(\frac{100 \text{ GeV}}{M_2} \right)^5 \left(\frac{10^{-3}}{y_2} \right)^2 \quad (20)$$

where we take $m_H = m_{H^\pm} \approx m_{H^0}$. This decay-length is orders of magnitude larger than the size of the detector and can not be probed at the moment.³ Therefore, the experimental signal of Scenario B consists in the observation of two prompt charged leptons and missing energy, from the production of a $H^+ H^-$ pair, followed by the decay $H^\pm \rightarrow N_2 \ell_\alpha^\pm$. A similar signature arises in simplified models of Supersymmetry with light sleptons and weakly-decaying charginos, which has been searched for by the ATLAS collaboration in [29]. We

³This could change in the future if the recently proposed MATHUSLA surface detector [28], which has the potential to add sensitivity to particles with $c\tau \gtrsim 10$ m to the existing LHC program, is built.

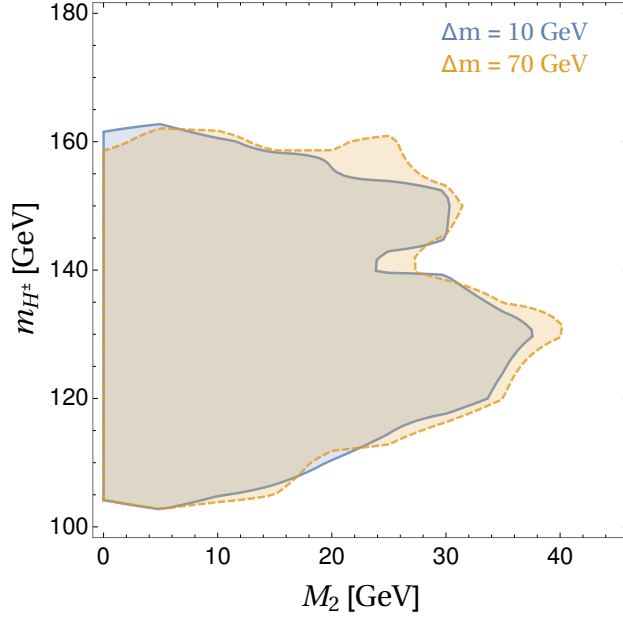


Figure 5: Parameter space of the Scenario B excluded by the ATLAS search for dileptons and missing energy [29] for $\Delta m_{\text{nc}} = 10$ GeV (blue) and $\Delta m_{\text{nc}} = 70$ GeV (yellow), assuming $\text{BR}(H^\pm \rightarrow N_2 \mu^\pm) = \text{BR}(H^\pm \rightarrow N_2 e^\pm) = 1/2$ and $\text{BR}(H^\pm \rightarrow N_2 \tau^\pm) = 0$.

simulate the production and decay of pairs of the scalars $H^\pm/A^0/H^0$ with CalcHEP [24] and pass the result to Pythia [25] for showering and hadronization. Finally, we use the recast of the experimental analysis implemented in Checkmate [30] which uses Delphes [26] to simulate detector effects.⁴

The analysis presented in [29] considers only final states with muons or electrons. As a result, the exclusion limits will show a strong dependence on the branching ratio into taus. We then consider two cases: *i*) an optimistic scenario in which the decays into taus are negligible and *ii*) a more conservative benchmark with $\text{BR}(H^\pm \rightarrow N_2 e^\pm) = \text{BR}(H^\pm \rightarrow N_2 \mu^\pm) = \text{BR}(H^\pm \rightarrow N_2 \tau^\pm) = 1/3$. As can be seen in Fig. 5, for the optimistic case the LHC probes a significant region of the parameter space and is able to exclude $m_{H^\pm} \lesssim 160$ GeV for light N_2 . In contrast, we find that once $\text{BR}(H^\pm \rightarrow N_2 \tau^\pm)$ is equal or larger than the branching ratio into electrons and muons, the whole parameter space becomes allowed.

3.3 Scenario C: $M_1 < M_2 < M_3 < m_{H^0, A^0, H^\pm}$

The scenario where all the Z_2 -odd fermions are lighter than the Z_2 -odd scalars produces two different signatures. The first signature arises from the decay $H^\pm \rightarrow N_2 \ell_\alpha^\pm$, which produces two charged leptons plus missing energy and, as N_2 has a long decay-length, this signal is identical to the one already discussed in Scenario B. The second signature arises from the decay $H^\pm \rightarrow N_3 \ell_\alpha^\pm$. In contrast to N_2 which is stable within the detector, N_3 can decay fast enough into $\ell_\alpha \bar{\ell}_\beta N_2$ to produce observable signals. The decay rate reads, assuming

⁴In Checkmate the ATLAS search [29] is available as an unvalidated analysis. To check the implementation we re-derived the limits on slepton production and find good agreement between the Checkmate result and the experimental analysis.

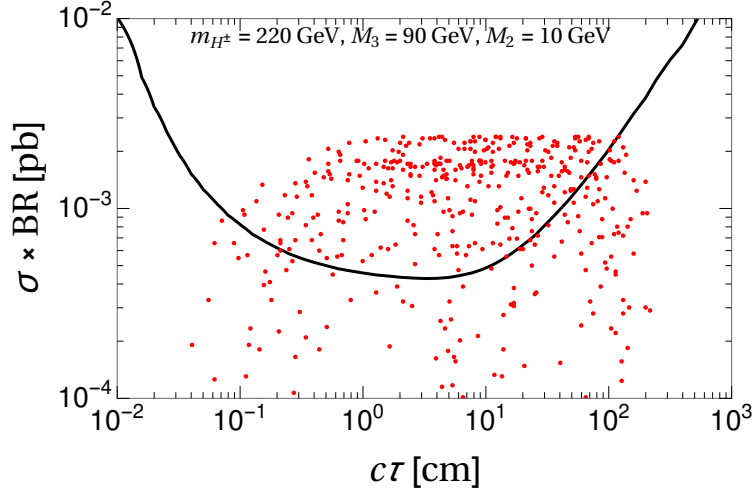


Figure 6: Cross-section times branching ratio into the $\mu^+\mu^-$ channel as a function of the proper decay-length $c\tau(N_3)$ for one exemplary choices of the scalar and right-handed neutrino masses in Scenario C. The solid black line corresponds to the 95% CL exclusion derived from the CMS limits on displaced dileptons.

$$M_2 \ll M_3,$$

$$\Gamma(N_3 \rightarrow \ell_\alpha^- \ell_\beta^+ N_2) \simeq \frac{M_3^5}{6144 \pi^3 m_{H^\pm}^4} \left(|Y_{\beta 2}^\nu|^2 |Y_{\alpha 3}^\nu|^2 + |Y_{\alpha 2}^\nu|^2 |Y_{\beta 3}^\nu|^2 \right), \quad (21)$$

Taking $m_H = m_{H^\pm} \approx m_{H^0}$ again, the proper decay-length of N_3 is

$$c\tau(N_3) \approx 0.4 \text{ m} \left(\frac{100 \text{ GeV}}{M_3} \right) \left(\frac{m_H}{M_3} \right)^4 \left(\frac{10^{-3}}{y_2} \right)^2 \left(\frac{10^{-3}}{y_3} \right)^2 \quad (22)$$

and can be macroscopic for some choices of the parameters of the model. Such displaced dilepton pairs are a very clean observable and can be searched for very efficiently at the LHC, see e.g. [31, 32]. Since limits on electron-positron pairs are typically a factor of a few weaker than those related to muons, we focus on the search for displaced dimuons presented in [32] and recast the limits reported by CMS to our model. For a description of the dilepton search and our treatment of the detector performance, we refer the reader to Appendix B.

The sensitivity of the experimental search is dictated by the dimuon production rate, which in turn depends on the H^\pm production cross-section times the branching ratio $\text{BR}(N_3 \rightarrow \mu^+\mu^- N_2)$, and by the displacement of the dimuon vertex from the collision point, which depends on the N_3 decay-length. We show in Fig. 6 the limits on the cross-section times branching ratio as a function of the proper decay-length $c\tau$ that we obtain from recasting the CMS results to this scenario. The excluded cross-section is fairly insensitive to the precise value of the proper decay-length in the range $0.1 - 10$ cm, while for larger and smaller values there is a rapid decrease of the sensitivity, since only a small fraction of the particles will decay in the tracker. To assess the impact of this search on the FIMP scotogenic model, we also show in the plot the predicted values of $\sigma \times \text{BR}$ and $c\tau$ obtained from a random scan of the Yukawa couplings of the model, and fixing for illustration $m_{H^\pm} = 220$ GeV,

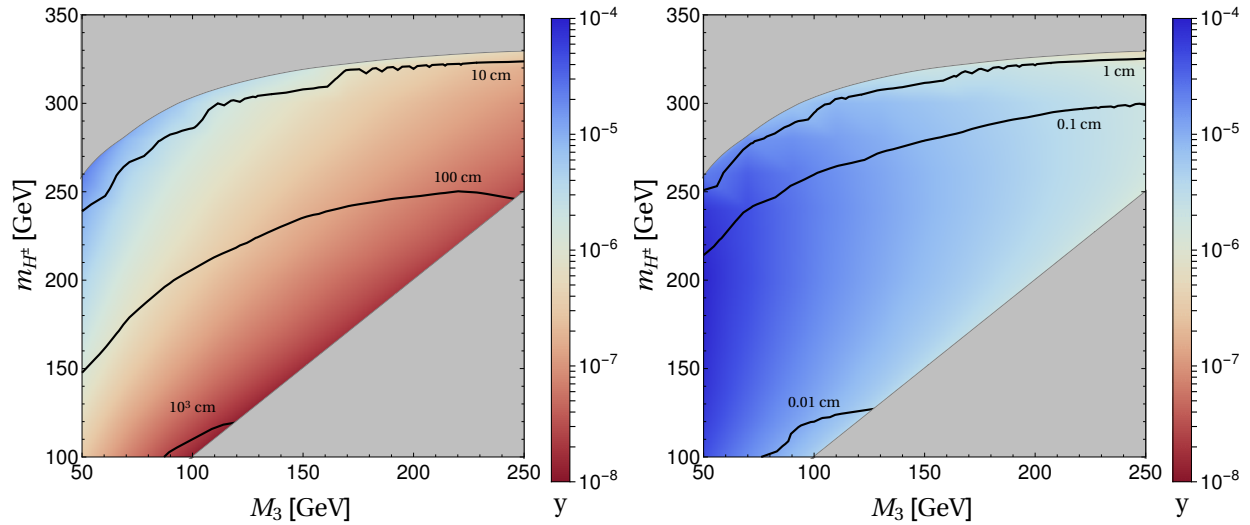


Figure 7: Smallest (left panel) and largest (right panel) combination of Yukawa couplings y excluded by current displaced dimuon searches at CMS in Scenario C, assuming $\text{BR}(N_3 \rightarrow \mu^+ \mu^- N_2) = 1/18$ and $M_2 = 10$ GeV. The black contour lines indicate the excluded proper decay-length $c\tau$. In the upper grey region the production rate is too low to allow an exclusion for any decay-length, whereas the lower grey region is kinematically inaccessible.

$M_3 = 90$ GeV and $M_2 = 10$ GeV. The Yukawa couplings were constructed, following the approach introduced in [33], such that they lead to the observed neutrino mass splittings and mixing angles. Furthermore, it was checked that all the points in the scan are in agreement with the upper limit on $\text{BR}(\mu \rightarrow e\gamma)$. As seen from the plot, a significant fraction of the parameter space of the model can be probed in searches for displaced muon pairs.

Conversely, one can use the CMS null results to constrain the fundamental parameters of the model relevant for this search, which are m_{H^\pm} , M_3 , M_2 and $|Y_{\mu 2}^\nu Y_{\mu 3}^\nu|$. Under the simplifying assumption $M_2 \ll M_3$ and fixing $\text{BR}(N_3 \rightarrow \mu^+ \mu^- N_2) = 1/18$, which is a reasonable expectation for an anarchic Yukawa matrix with similar couplings to all flavours, the free parameters of the model reduce to m_{H^\pm} , M_3 and $y \equiv \sqrt{|Y_{\mu 2}^\nu Y_{\mu 3}^\nu|}$. It is easy to see that, for fixed values of m_{H^\pm} and M_3 , the CMS search can set a lower and an upper limit on y : for smaller values of y , N_3 becomes long-lived compared to the detector scales, while for larger values, N_3 decays too fast and does not leave a displaced dimuon signal. The lower and upper limits of y in the M_3 - m_{H^\pm} plane are shown in Fig. 7. The black lines in the plots represent the limit on the proper decay-length of N_3 .

4 Conclusions

We analysed a scenario where the dark matter candidate is the lightest fermion singlet of the scotogenic neutrino mass model, under the assumption that the present dark matter abundance is generated via the freeze-in mechanism. The small interaction strength of N_1 required to correctly reproduce the observed dark matter abundance implies very suppressed decay rates of the next-to-lightest Z_2 -odd particle, which translate into macroscopic decay-

lengths.

We have investigated possible signals of this model in three representative scenarios, characterized by the spectra of the Z_2 -odd particles. Each spectrum leads to very characteristic signatures at the Large Hadron Collider, which lead to different constraints on the model parameters:

- Scenario A: $M_1 < m_{H^\pm, H^0, A^0} < M_{2,3}$. The charged component of the Z_2 -odd scalar doublet, H^\pm , is long-lived and leaves a highly ionizing charged track in the detector. For $M_1 \gtrsim 1$ MeV, most of the produced charged scalars leave the detector, producing a long track; the non-observation of this signal at the LHC excludes $m_{H^\pm} \lesssim 500$ GeV. On the other hand, for lighter dark matter, the proper decay-length becomes comparable or smaller than the size of the detector. In this case, the sensitivity of the search decreases. Nevertheless, we still find significant constraints on the parameter space, namely we find $m_{H^\pm} \gtrsim 400$ GeV (200 GeV) for $M_1 = 100$ keV (10 keV). For $M_1 \lesssim 1$ keV, the charged scalar decays fast and does not leave any observable track. Furthermore, for $M_1 \gtrsim 1$ MeV, a fraction of the produced charged scalars is stopped in the detector and may decay in the time interval in which there is no bunch crossing. We find that, unfortunately, current limits on this class of exotic events are not strong enough to constrain this model.
- Scenario B: $M_1 < M_2 < m_{H^\pm, H^0, A^0} < M_3$. In this scenario, the charged scalar decays promptly to N_2 and a charged lepton, producing a signature consisting of hard leptons and missing energy. We find that, when N_2 couples mostly to the electron or the muon flavour, charged scalar masses up to ≈ 160 GeV can be excluded.
- Scenario C: $M_1 < M_2 < M_3 < m_{H^\pm, H^0, A^0}$. In this case, the non-observation of the process $\mu \rightarrow e\gamma$ translates into small Yukawa couplings of N_3 and N_2 to the charged leptons, which in turn translates into a rather small width for the decay $N_3 \rightarrow \ell_\alpha^- \ell_\beta^+ N_2$. As a result, this scenario can be probed by searching for displaced dileptons at the LHC. Notably, and in contrast to the other two scenarios, if this one is realized in Nature, it may be possible to directly probe the parameters responsible for neutrino masses. We find that current searches for displaced dimuons at CMS already probe regions of the parameter space allowed by other searches and set quite stringent constraints on the size of the Yukawa couplings.

The FIMP realization of the scotogenic model presents a rich phenomenology which can be probed using various searches for long-lived particles at the LHC. The model could then serve as a proxy to assess the impact of these searches for concrete Particle Physics models. Given the possible relevance of this searches for understanding the nature of the dark matter and the origin of neutrino masses, we would like to encourage the experimental collaborations to strengthen their efforts in conducting searches for long-lived particles, especially in association with energetic leptons in the final state. Finally, it should be noted that new detectors specifically designed to address the problems posed by long-lived particles, for example the proposed MATHUSLA experiment [28], could extend the sensitivity well beyond the range currently probed at the LHC.

5 Acknowledgements

This work was supported in part by the DFG cluster of excellence EXC 153 “Origin and Structure of the Universe”. The CP3-Origins center is partially funded by the Danish National Research Foundation, grant number DNR90. A. G. H. was supported by Fundação para a Ciência e a Tecnologia (FCT) through the grant SFRH/BD/76052/2011, financed by the European Social Fund (ESF) through POPH under the QREN framework.

A Stopped particles

The stopped particles analysis requires a realistic description of the ATLAS detector and the energy losses therein, which depend crucially on the material properties. The mean energy loss of particles in a given material is described by the Bethe-Bloch equation [34],

$$\langle -dE/dx \rangle = \kappa z^2 \langle Z/A \rangle \rho \frac{1}{\beta^2} \left[\ln \left(\frac{2 m_e}{I} \frac{E^2 - M^2}{M \sqrt{M^2 + 2 m_e E + m_e^2}} \right) - \beta^2 \right], \quad (23)$$

where E is the energy, M is the mass, z the electric charge and $\beta = v/c$, with v being the velocity of the particle. The constant κ has the value $0.307 \text{ MeV g}^{-1} \text{ cm}^2$. The quantities ρ , I , Z and A , describe the material and represent the density, mean excitation energy, atomic number and atomic weight of the medium, respectively. $\langle Z/A \rangle$ is the mean weighted over isotopic abundances on Earth. These quantities are not constant throughout the detector but vary along the path of the particles. Given that the experimental search [22] only considers events with $|\eta| < 1.2$ it is sufficient to consider the barrel. In the following we briefly describe the simplified detector used in our analysis. A summary of the detector geometry and the material constants can be found in Tab. 1 ⁵.

To incorporate the cylindrical geometry, we define the material constants in terms of box functions of the distance from the interaction point x and of the pseudorapidity η . The solenoid (Sol.), the muon system (MS) and the toroid (Tor.) of ATLAS have a low density and we neglect them in our treatment of the energy losses. Significant energy losses occur in the electromagnetic calorimeter (ECAL) and the hadron calorimeter (HCAL) composed by the long (HLB) and extended barrel (HEB) modules in the region of interest. Particles which pass the calorimeters will not contribute to the stopped particle signal. The calorimeters are not homogeneous slabs of material and, therefore, the material coefficients entering the Bethe-Bloch equation need to be averaged over the different components. For compound materials, we use the Bragg additivity rule [39], i.e. we sum the different $\log(I)$ and Z/A of the various materials weighted by their respective mass fraction.

The ECAL barrel, which is part of the liquid argon (LAr) calorimeter system, is subdivided into two regions with different LAr and lead (Pb) proportions; these pseudorapidity ranges are denoted by R1 and R2 in Tab. 1. The geometry and composition of the various ECAL layers is not simple enough to allow for an easy determination of an effective average density. ATLAS sources [40, 41] apply a method with an “effective molecule” with numbers

⁵The information on geometry and material properties was extracted from the official technical descriptions of the ATLAS experiment [35] and from publicly available technical design reports (TDRs) [36, 37, 38]. Numerical values for the material constants are taken from the PDG [34], unless otherwise specified in the TDRs.

Layer	Δ [cm]	$[\eta _{\min}, \eta _{\max}]$	Material	$\langle \rho \rangle$ [g/cm ³]	$\langle I \rangle$ [eV]	$\langle Z/A \rangle$
ID+Sol.	150.0	[0, 1.4]	Vacuum	-	-	-
EMB R1	47.6	[0, 0.8]	LAr+Pb	4.01	487	0.406
EMB R2	47.6	[0.8, 1.4]	LAr+Pb	3.67	447	0.408
HLB+HEB	197.0	[0, 1.4]	Fe+PS	6.40	286	0.466
MS+Tor.	∞	[0, 1]	Vacuum	-	-	-

Table 1: Specs of our simplified ATLAS barrel. See the text for details.

of representative atoms chosen to reproduce the overall proportions of lead, reinforcing steel and argon. For the ECAL barrel in the region R1, this is stated to yield a density of 4.01 g/cm³. We use the same molecule combined with Bragg additivity to compute the effective density for the other region, with atom numbers in the chemical formula adjusted by factors obtained from the different thicknesses of the absorber and radiator layers. Moreover, we also apply the Bragg rule to compute the means of I and Z/A . In the HCAL, 82% of the volume is made up by iron while the rest is taken by plastic scintillators. We once again use the Bragg additivity rule to perform the material averages.

With these ingredients we can solve the Bethe-Bloch equation and, since energy losses are treated as continuous, we get, for each direction in the detector, a maximal value of β for which the charged particles stop. The stopping efficiency ϵ_{stop} is then given by

$$\epsilon_{\text{stop}}(\tau) = \int_{|\eta| < 1.2} d\eta \int_1^{\beta\gamma_{\text{lim}}(\eta)} d\beta\gamma \frac{1}{\sigma} \frac{d^2\sigma}{d\beta\gamma d\eta} P_{\text{sur}}(\beta\gamma, \eta). \quad (24)$$

We perform the integration over the pseudorapidity range considered in the experimental analysis and up to the maximum value $\beta\gamma_{\text{lim}}(\eta)$ at the point of production for which the particle with pseudorapidity η gets trapped in the ECAL or the HCAL. This value is given by the solution of the Bethe-Bloch equation. Lastly, P_{sur} accounts for the instability of the H^\pm particles, namely it corresponds to the probability to survive until the particle is stopped. However, this factor is only relevant for very short lifetimes which can not be probed at the LHC due to the vanishing timing efficiency $\epsilon_T(\tau)$, hence we take $P_{\text{sur}} = 1$ in our analysis.

B Displaced dileptons

The CMS displaced dilepton analysis [32] searches for pairs of electrons or muons originating from a secondary vertex with a substantial separation from the collision point. As the limits on muon pairs are considerably stronger than the ones for electrons we will focus our attention on the muon channel. The detector model used in our analysis follows roughly the phenomenological recast described in [42].

The first ingredient for a reinterpretation of the CMS analysis is a description of the detector and the efficiencies with which tracks originating from displaced vertices can be observed. Unfortunately, the performance of the CMS tracker is not publicly known in detail and we have to work with some simplified approximations. In the following we assume that the tracker is close to perfect and that the tracking efficiency depends exclusively on the position of the displaced vertex. Motivated by Fig. 3 of [32] we model the dependence

of the tracker efficiency on the transverse displacement $|d_0|$ as a broken linear function. Our efficiency starts at 1 for $d_0=0$, falls to 0.8 at $|d_0| = 15$ cm and drops to 0 for $|d_0| \geq 30$. We take a similar approach for the longitudinal displacement $|z_0|$. Here the efficiency falls to 0.8 at $|z_0| = 30$ cm before dropping to 0 for $|z_0| \geq 55$ cm. Following [42] we require a hard cut on the radial displacement r and set the tracking efficiency to zero for $r \geq 60$ cm.

Once the probability for the detection of a lepton pair has been determined, we have to make sure that the event passes the experimental cuts for dilepton candidates. Both muons must have a $p_T > 26$ GeV in order to be sufficiently above the trigger threshold of 23 GeV. The pseudorapidity of $|\eta| < 2$ is required in order to ensure that the leptons are observed in the well-instrumented region of the tracker. A cut on the total invariant mass of the lepton pair $m_{\ell\ell} > 15$ GeV suppresses a possible contamination from meson decays. In addition, a minimal separation of the two muon tracks of $\Delta R > 0.2$ is required to ensure a high dimuon trigger efficiency. The absolute difference in azimuthal angle $|\Delta\Phi|$ between the displaced vertex and the momentum of the dilepton has to be smaller than $\pi/2$. Finally, the tracks have to exhibit a significant transverse displacement $|d_0|$ from the primary vertex of more than 12σ , where σ is the uncertainty of d_0 . Since this uncertainty is not accessible without a full detector simulation we replace this condition with a minimal displacement $|d_0| > 250 \mu\text{m}$. The expected number of background events in this search is zero and, since no events were observed, $N = 3$ is excluded at 95% CL.

In order to check the validity of our analysis we have rederived the CMS limits for some of the representative benchmark scenarios presented in [32]; our results agree with those from CMS within 30%.

References

- [1] G. Bertone *et al.*, Cambridge, UK: Univ. Pr. (2010) 738 p
- [2] L. Bergström, Rept. Prog. Phys. **63** (2000) 793 doi:10.1088/0034-4885/63/5/2r3 [hep-ph/0002126].
- [3] G. Bertone, D. Hooper and J. Silk, Phys. Rept. **405** (2005) 279 doi:10.1016/j.physrep.2004.08.031 [hep-ph/0404175].
- [4] H. Baer, K. Y. Choi, J. E. Kim and L. Roszkowski, Phys. Rept. **555** (2015) 1 doi:10.1016/j.physrep.2014.10.002 [arXiv:1407.0017 [hep-ph]].
- [5] S. S. Gershtein and Y. B. Zeldovich, JETP Lett. **4** (1966) 120 [Pisma Zh. Eksp. Teor. Fiz. **4** (1966) 174].
- [6] P. A. R. Ade *et al.* [Planck Collaboration], Astron. Astrophys. **571** (2014) A16 doi:10.1051/0004-6361/201321591 [arXiv:1303.5076 [astro-ph.CO]].
- [7] L. J. Hall, K. Jedamzik, J. March-Russell and S. M. West, JHEP **1003** (2010) 080 doi:10.1007/JHEP03(2010)080 [arXiv:0911.1120 [hep-ph]].
- [8] E. Ma, Phys. Rev. D **73** (2006) 077301 doi:10.1103/PhysRevD.73.077301 [hep-ph/0601225].

- [9] E. Ma, Mod. Phys. Lett. A **21** (2006) 1777 doi:10.1142/S0217732306021141 [hep-ph/0605180].
- [10] J. Kubo, E. Ma and D. Suematsu, Phys. Lett. B **642** (2006) 18 doi:10.1016/j.physletb.2006.08.085 [hep-ph/0604114].
- [11] E. Molinaro, C. E. Yaguna and O. Zapata, JCAP **1407** (2014) 015 doi:10.1088/1475-7516/2014/07/015 [arXiv:1405.1259 [hep-ph]].
- [12] G. Aad *et al.* [ATLAS Collaboration], Phys. Lett. B **716** (2012) 1 doi:10.1016/j.physletb.2012.08.020 [arXiv:1207.7214 [hep-ex]].
- [13] S. Chatrchyan *et al.* [CMS Collaboration], Phys. Lett. B **716** (2012) 30 doi:10.1016/j.physletb.2012.08.021 [arXiv:1207.7235 [hep-ex]].
- [14] T. Hambye, F.-S. Ling, L. Lopez Honorez and J. Rocher, JHEP **0907** (2009) 090 Erratum: [JHEP **1005** (2010) 066] doi:10.1007/JHEP05(2010)066, 10.1088/1126-6708/2009/07/090 [arXiv:0903.4010 [hep-ph]].
- [15] I. F. Ginzburg and I. P. Ivanov, hep-ph/0312374.
- [16] T. Toma and A. Vicente, JHEP **1401** (2014) 160 doi:10.1007/JHEP01(2014)160 [arXiv:1312.2840, arXiv:1312.2840 [hep-ph]].
- [17] A. M. Baldini *et al.* [MEG Collaboration], arXiv:1605.05081 [hep-ex].
- [18] A. Ibarra, C. E. Yaguna and O. Zapata, Phys. Rev. D **93** (2016) no.3, 035012 doi:10.1103/PhysRevD.93.035012 [arXiv:1601.01163 [hep-ph]].
- [19] J. L. Feng, A. Rajaraman and F. Takayama, Phys. Rev. Lett. **91** (2003) 011302 doi:10.1103/PhysRevLett.91.011302 [hep-ph/0302215].
- [20] A. G. Hessler, A. Ibarra, E. Molinaro and S. Vogl, Phys. Rev. D **91** (2015) no.11, 115004 doi:10.1103/PhysRevD.91.115004 [arXiv:1408.0983 [hep-ph]].
- [21] S. Chatrchyan *et al.* [CMS Collaboration], JHEP **1307** (2013) 122 doi:10.1007/JHEP07(2013)122 [arXiv:1305.0491 [hep-ex]].
- [22] G. Aad *et al.* [ATLAS Collaboration], Phys. Rev. D **88** (2013) no.11, 112003 doi:10.1103/PhysRevD.88.112003 [arXiv:1310.6584 [hep-ex]].
- [23] V. Khachatryan *et al.* [CMS Collaboration], Eur. Phys. J. C **75** (2015) no.7, 325 doi:10.1140/epjc/s10052-015-3533-3 [arXiv:1502.02522 [hep-ex]].
- [24] A. Belyaev, N. D. Christensen and A. Pukhov, Comput. Phys. Commun. **184** (2013) 1729 doi:10.1016/j.cpc.2013.01.014 [arXiv:1207.6082 [hep-ph]].
- [25] T. Sjostrand *et al.*, Comput. Phys. Commun. **191** (2015) 159 doi:10.1016/j.cpc.2015.01.024 [arXiv:1410.3012 [hep-ph]].
- [26] J. de Favereau *et al.* [DELPHES 3 Collaboration], JHEP **1402** (2014) 057 doi:10.1007/JHEP02(2014)057 [arXiv:1307.6346 [hep-ex]].

- [27] G. J. Feldman and R. D. Cousins, Phys. Rev. D **57** (1998) 3873 doi:10.1103/PhysRevD.57.3873 [physics/9711021 [physics.data-an]].
- [28] J. P. Chou, D. Curtin and H. J. Lubatti, arXiv:1606.06298 [hep-ph].
- [29] G. Aad *et al.* [ATLAS Collaboration], JHEP **1405** (2014) 071 doi:10.1007/JHEP05(2014)071 [arXiv:1403.5294 [hep-ex]].
- [30] M. Drees, H. Dreiner, D. Schmeier, J. Tattersall and J. S. Kim, Comput. Phys. Commun. **187** (2014) 227 doi:10.1016/j.cpc.2014.10.018 [arXiv:1312.2591 [hep-ph]].
- [31] V. Khachatryan *et al.* [CMS Collaboration], Phys. Rev. Lett. **114** (2015) no.6, 061801 doi:10.1103/PhysRevLett.114.061801 [arXiv:1409.4789 [hep-ex]].
- [32] V. Khachatryan *et al.* [CMS Collaboration], Phys. Rev. D **91** (2015) no.5, 052012 doi:10.1103/PhysRevD.91.052012 [arXiv:1411.6977 [hep-ex]].
- [33] J. A. Casas and A. Ibarra, Nucl. Phys. B **618** (2001) 171 doi:10.1016/S0550-3213(01)00475-8 [hep-ph/0103065].
- [34] K. A. Olive *et al.* [Particle Data Group Collaboration], Chin. Phys. C **38** (2014) 090001. doi:10.1088/1674-1137/38/9/090001
- [35] G. Aad *et al.* [ATLAS Collaboration], JINST **3** (2008) S08003. doi:10.1088/1748-0221/3/08/S08003
- [36] [ATLAS Collaboration], CERN-LHCC-96-41.
- [37] [ATLAS Collaboration], CERN-LHCC-96-42.
- [38] [ATLAS Collaboration], CERN-LHCC-97-22, ATLAS-TDR-10.
- [39] D. E. Groom, N. V. Mokhov and S. I. Striganov, Atom. Data Nucl. Data Tabl. **78** (2001) 183. doi:10.1006/adnd.2001.0861
- [40] M. Aourousseau, CERN-THESIS-2010-138, LAPP-T-2010-05.
- [41] A. A. Abdelalim, CERN-THESIS-2008-151.
- [42] Z. Liu and B. Tweedie, JHEP **1506** (2015) 042 doi:10.1007/JHEP06(2015)042 [arXiv:1503.05923 [hep-ph]].